Engineering ultrastrong coupling between Josephson plasmon polaritons and subwavelength microcavity arrays in silicon/van der Waals layered superconductor heterostructure for terahertz hybrid circuit cavity quantum electrodynamics

Samane Kalhor,[1] Sergey Savel'ev [2] and Kaveh Delfanazari [1,*]

[1]*Electronics and Nanoscale Engineering Division, James Watt School of Engineering, University of Glasgow, Glasgow G12 8QQ, United Kingdom*
[2]*Department of Physics, Loughborough University, Loughborough LE11 3TU, United Kingdom*

The realization of the ultrastrong coupling between Josephson plasma waves (JPWs) and terahertz (THz) photons in the subwavelength microcavity array is of interest for manipulating the THz cavity quantum electrodynamics (cQED), ultrahigh-resolution sensing and imaging, and quantum information processing. Here, we describe the engineering of ultrastrong light-matter interactions in a deeply subwavelength microcavity array based on the hybrid silicon and high-temperature superconductor (HTS) $Bi_2Sr_2CaCu_2O_{8+\delta}$ (BSCCO) van der Waals (vdW) heterostructure. We perform numerical modeling and analytical calculation to describe Josephson THz cQED and the ultrastrong coupling process between THz radiation and the JPWs in Josephson medium which is naturally present in BSCCO vdW. The resonance frequency of microcavities is swept through the Josephson plasma frequency by altering their width. THz reflection demonstrates the anticrossing behavior of ultrastrong coupling with a normalized Rabi frequency (coupling strength) $2\Omega_R/f_c = 0.29$ for the BSCCO thickness $t = 200$ nm, which increases to the value of 0.87 for $t = 800$ nm. Furthermore, the thermal behavior of coupling strength shows modulation of Rabi splitting $2\Omega_R$ with temperature. We show that the normalized Rabi splitting $2\Omega_R/f_c$ is independent of the temperature in the BSCCO superconducting regime, while a weak coupling can be observed above the superconducting transition temperature. The proposed chip-scale THz photonic integrated circuit with subwavelength microcavity metamaterial array shall guide the effort in the development of power-efficient coherent THz sources, quantum sensors, ultrasensitive detectors, parametric amplifiers and tunable bolometers based on BSCCO HTS quantum material.

I. INTRODUCTION

Terahertz (THz) radiation advances both fundamental sciences and technological applications [1–4]. Some examples are the discovery of material properties through THz light-matter interactions, THz off/on-chip sensing, spectroscopy, high-resolution imaging, tomography, and high-speed wireless communication [1]. Specifically, THz electromagnetic (EM) waves can be applied to investigate the superconducting condensate in the layered high-temperature superconductors (HTSs) [2,4–6]. In the category of HTS, $Bi_2Sr_2CaCu_2O_{8+\delta}$ (BSCCO) based devices have shown a potential to close the THz gap [7–11]. The crystal of HTS BSCCO is a stack of two-dimensional (2D) layers composed of alternating layers of superconducting copper oxides (CuO_2) and nonsuperconducting bismuth/strontium oxides (Bi_2O_2 and SrO) forming intrinsic Josephson junctions (IJJs) or Josephson medium [12–15]. Therefore, superconductivity in BSCCO is confined to 2D planes [16] and the relatively weak van der Waals (vdW) forces between the layers keep the stack together [17]. The atomically thin BSCCO layers can be obtained through the exfoliation of bulk BSCCO. Cleaving down to a few BSCCO layers can be used for the investigation of the origin of strong correlations and 2D superconductivity, the electronic properties of HTS [18], and surface studies [19]. The Josephson current along the crystallographic c-axis of BSCCO can couple with the EM waves and produce the Josephson plasma waves (JPWs) [20]. JPWs have been investigated for many applications including solid-state quantum emitters, coherent detectors, filters, and waveguides [21–23]. One focus in this field is on nonlinear JPWs which offer the remarkable nonlinear phenomenon of the slowing down of light, self-induced transparency, pumping of a weak wave by a strong wave, and conversion of continuous THz radiation into short strong THz pulses [24]. Another interest in JPWs is caused by the Josephson plasma resonance. It is the resonant interaction of JPWs with an external microwave electric field and it is a powerful tool to provide information about the Josephson coupling and the vortex phase in layered superconductors [25]. Moreover, the interface between the vacuum and the superconductor supports the propagation of the surface JPWs and provides significant suppression of the reflection (Wood-like anomalies) that can be used in THz filters [26]. In addition, the triangular lattice form of Josephson vortices, which arises due to an external dc applied magnetic field parallel to the

*kaveh.delfanazari@glasgow.ac.uk

crystallographic *ab*-plane of the superconductors, is in analogy with optical photonic crystals. Therefore, these Josephson vortex crystals exhibit noteworthy features including band gaps and tunable transparency [27]. A main and fascinating feature of JPWs is the coherent and continuous THz waves radiation by exciting the uniform Josephson oscillations which results in emerging coherent and power-efficient THz sources, called IJJ quantum emitters, over the past decade [28–34]. These emitters have a considerably larger frequency range tunability compared to the other solid-state THz sources [35–37]. In addition, as a result of weak vdW force between BSCCO layers, exfoliation to a small volume, and transferring to any desired substrate, BSCCO is a good material candidate for ultrasensitive sensors [38] and detectors with a lower response time constant [39]. Consequently, the BSCCO-based devices, capable of operation above liquid nitrogen temperature, are used in a wide range of frequencies from microwave [40], to THz [41,42], and visible-near infrared [38]. As a result, it would be very desirable to excite the EM waves in BSCCO in a controllable way. Strong light-matter coupling can control the macroscopic systems and manipulate the energy spectrum of the Josephson plasmon and applied THz EM waves. Light-matter interaction is the process of periodically exchanging energy between matter and light [43–45]. Due to the overcoming of strong coupling to the dissipation rate of the system, it enables the coherent oscillation of Josephson waves. Therefore, a strong emission power can be obtained by coherent phase synchronization of the Josephson current between different Josephson junctions in BSCCO [46–48]. The strong light-matter coupling also results in the cooling of superconducting order parameter phase fluctuations and helps in reducing the loss near the transition temperature for more powerful radiation [49].

Strong coupling was reported in different systems including the intersubband transition of quantum well [50], two-dimensional electron gas (2DEG) [51], surface plasmon polariton [43], superconducting qubits [52], and cuprates [49,53]. The resonators for coupling fall into three categories of metamaterials [54], microcavities [55], and quantum materials [56]. The subwavelength confinement of the light in double-metal microcavities results in an ultrastrong light-matter coupling [50].

In this paper, we propose a method that leads to ultrastrong coupling between the JPWs in BSCCO and the resonance of the deeply subwavelength microcavity array. The gap between the two gold metals is filled with a sandwich structure of hybrid silicon/BSCCO/silicon. Silicon is chosen as it is the main pillar of the optoelectronic for the implementation of generation, modulation, and detection [57]. It facilitates the integration of THz devices with silicon photonics technology for the realization of all integrated photonics chips. In the long term, the proposed devices will benefit from the remarkable optical properties of silicon such as ultrafast terahertz optical response [58] and nonlinearity [59].

The round trip of a photon bouncing between two metals of each microcavity permits the interaction of Josephson plasmon to the EM waves which results in the appearance of hybridized modes split by the Rabi frequency. Here, the coupling strength of the system is carried out for different temperatures ranging from $T = 20$ K to above the BSCCO
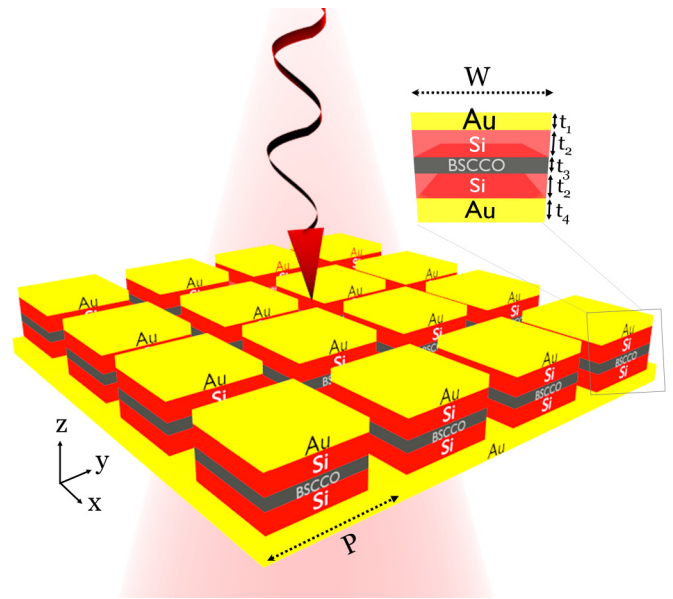
FIG. 1. The proposed THz cavity quantum electrodynamic (cQED) with arrays of subwavelength hybrid silicon (Si)-BSCCO microcavity. Inset is the cavity resonator unit cell with gold (Au) (yellow, $t_1 = 200$ nm)/Si (red)/BSCCO (black)/Si (red)/Au (yellow, $t_4 = 500$ nm) and a period of $p = 100\,\mu$m. Cavity width w, silicon thickness t_2, and BSCCO thickness t_3 are varied (see text).

transition temperature (T_c). At $T = 20$ K, the system has the largest Rabi splitting which reduces with increasing temperature. The normalized Rabi splitting is independent of temperature below T_c even though Rabi splitting fades above T_c. Furthermore, the coupling strength is investigated for a different filling fraction of the superconductor in each microcavity. Rabi splitting increases with increasing the filling fraction. Our results may open new opportunities for manipulating BSCCO JPWs and the development of tunable quantum emitters and detectors based on BSCCO HTS material. An IJJ emitter based on this strong light-matter interaction benefits from the synchronization of the Josephson junctions as a result of the high-quality factor of cavity resonance and cooling of superconducting phase fluctuation to boost its radiated power [60]. In addition, the enhancement in the radiated power of IJJs in this system is expected due to the matching of Josephson frequency with cavity frequency [61–63]. Moreover, the enhancement of the electric field in the superconducting part of the cavity can also be beneficial for increasing the sensitivity of the THz detector based on BSCCO IJJs [64].

II. DESIGN OF MICROCAVITY ARRAY

Microcavities are applied to confine light, produce strong absorption of EM fields and a sharp dip in the reflection spectra. Each cavity has a topcoat of gold (thickness $t_1 = 200$ nm) and a gold back plane ($t_4 = 500$ nm). The distance between two gold layers is filled by a heterostructure of silicon/BSCCO/silicon. Figure 1 schematizes the geometry of every single cavity and the array in which the width w of the cavities sets the resonance frequency of the cavity
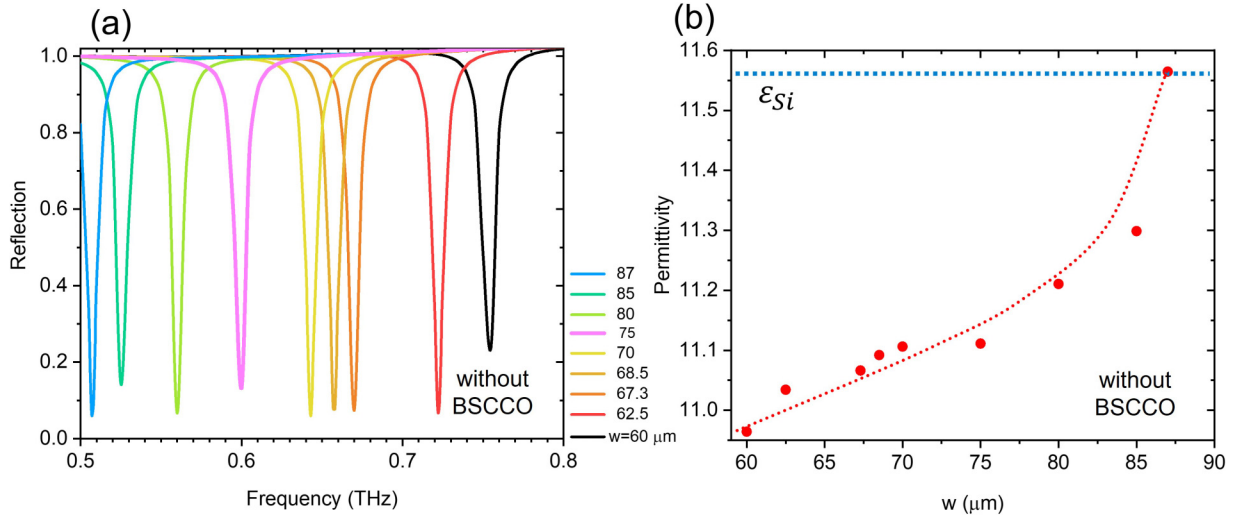
FIG. 2. (a) The simulated reflection spectra for different cavity width when there is no superconductor between silicon layers. (b) The calculated effective permittivity of the cavity. It asymptotically approaches the silicon permittivity ($\varepsilon_{\mathrm{si}}$) with increasing the cavity width. The red dotted line is a guide to the eye.

mode. The cavity array has a subwavelength spacing of $p = 100\,\mu$m. Here, BSCCO is set to be a c-axis oriented film (with $T_c = 90$ K). The plane THz wave is incident normally on the structure. The distance between two gold patches is kept constant as $t_3 + 2t_2 = 1200$ nm. The c-axis dielectric function of BSCCO can be defined as [65]

$$\varepsilon_{sc}(\omega) = \varepsilon_{\infty}\left(1 - f_p^2/f^2\right), \qquad (1)$$

where $\varepsilon_{\infty} = 12$, and f_p is the screened Josephson plasma frequency. The temperature dependent Josephson plasma frequency of BSCCO has been investigated in Ref. [66]; f_p is zero above T_c but rises sharply below T_c and saturates at about nearly $T_c/2$. It approaches $f_p = 0.67$ THz at $T = 20$ K. The complex permittivity of gold is calculated from a simple Drude model [67], and the permittivity of silicon is set to $\varepsilon_{si} = 11.56$ [68]. For investigation of the EM response of the presented device, a simulation is performed using the rf module of COMSOL Multiphysics [69].

III. RESULTS AND DISCUSSION

For characterization of the absorption resonance, cavities with different widths from $w = 60\,\mu$m to $w = 87\,\mu$m are studied when there is only silicon between the gold patches with no superconducting film. The reflection spectrum of cavity arrays is shown in Fig. 2(a). One dip is observed for each w which indicates the resonance frequency of the cavity arrays. The wavelength of the THz plane wave is much larger than the distance between two gold films ($\lambda \gg t_3 + 2t_2$). Therefore, a standing electromagnetic wave pattern is formed within two gold patches and the cavity supports two degenerate transverse magnetic modes TM$_{010}$ and TM$_{100}$. So, the resonance frequencies of the cavity follow the expression of

$$f_c = \frac{c}{2w\sqrt{\varepsilon_{\mathrm{eff}}}}\sqrt{n^2 + m^2 + l^2} = \frac{c}{2w\sqrt{\varepsilon_{\mathrm{eff}}}}, \qquad (2)$$

where c is the speed of light, w is the cavity width, and $\varepsilon_{\mathrm{eff}}$ is the effective permittivity of the standing wave in the cavity.

By knowing the width of the structure and the resonance frequencies, the effective permittivity is calculated from Eq. (2) and plotted in Fig. 2(b). The effective permittivity is different from the silicon permittivity, and it asymptotically approaches the silicon permittivity at width $w = 87\,\mu$m close to the unit cell period value $p = 100\,\mu$m.

IV. COUPLING STRENGTH AT $T = 20$ K

At first, we investigate the THz EM waves and BSCCO JPWs coupling at $T = 20$ K where $f_p = 0.67$ THz. Here, the cavity width is set to $w = 67.3\,\mu$m. Therefore, the bare cavity resonance frequency and JPWs are equal ($f_c = f_p$). To describe the coupling process, the reflection spectrum of the cavity array for two different configurations is shown in Fig. 3(a).
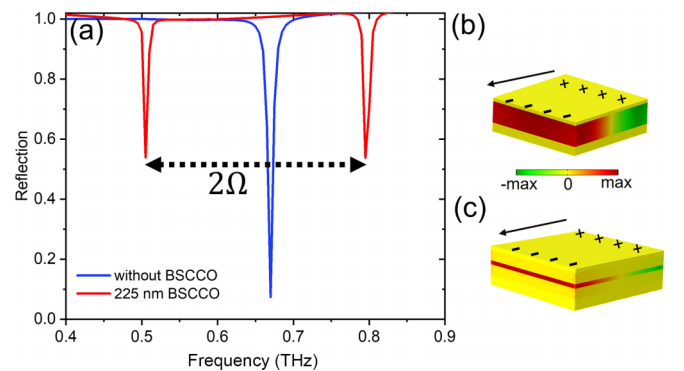
FIG. 3. (a) The reflection spectra for cavity width $w = 67.3\,\mu$m with only silicon (without superconducting BSCCO) is shown in blue, and with a BSCCO layer of thickness $t_3 = 225$ nm is shown in red. The z-component of the electric field when there is (b) no BSCCO, and (c) BSCCO with thickness $t_3 = 225$ nm, at $f = 0.67$ THz. The black arrows show the dipole moment. Here, Josephson plasma frequency is $f_p = 0.67$ THz (at $T = 20$ K).
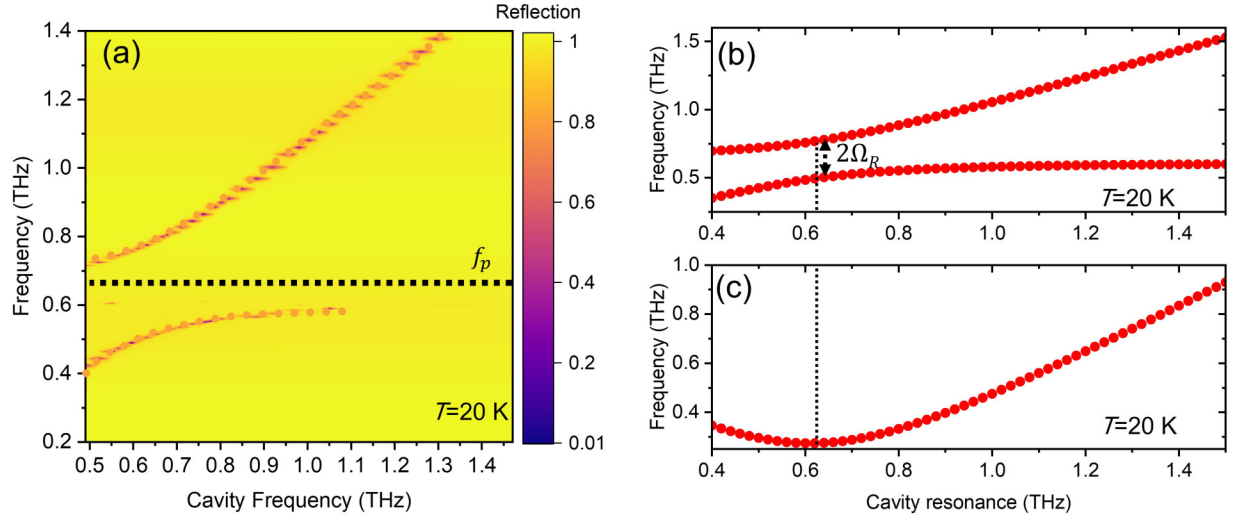
FIG. 4. (a) The color-coded reflection as a function of frequency and bare cavity frequency $f_c = c/(2\sqrt{\varepsilon_{si}}w)$. Here, w is set to vary from $w = 30$ to $90\,\mu$m. A dotted line is passed through the data as a guide to the eye. The black dashed line shows the BSCCO Josephson plasma frequency, (b) the theoretically calculated hybridized mode as a function of bare cavity frequency, (c) frequency splitting as a function of bare cavity frequency where the minimum value is the vacuum Rabi splitting. Here, thickness of BSCCO and silicon are set to $t_3 = 200$ nm and $t_2 = 500$ nm, respectively. The superconducting filling fraction is $F \sim 0.17$ and Josephson plasma frequency is $f_p = 0.67$ THz (at $T = 20$ K).

The blue line is the reflection of the condition where there is only silicon with a thickness of $t = 1200$ nm between two gold patches. No frequency splitting (strong coupling) is obtained. The red line shows the reflection when BSCCO with a thickness of $t_3 = 225$ nm is placed in the middle of silicon layers each with a thickness of $t_2 = 478.5$ nm. It is found that the reflection curve displays two dips with a frequency separation of 2Ω. This frequency splitting determines the strength of exchange coupling between the THz EM waves and Josephson plasmons. Two dips of reflection spectra correspond to the upper and lower hybridized states. The z-component of the electric field at $f = 0.67$ THz is plotted in Figs. 3(b) and 3(c) for the blue and red curves of Fig. 3(a), respectively. The charges with opposite signs are induced at the edge of the cavity. Therefore, the distribution of charge on the upper gold patch has a net dipole moment on the surface and it is parallel to the electric field of the applied EM wave [70]. A standing wave, independent of z, is localized in the silicon region [see Fig. 3(b)] due to ($\lambda \gg t_3 + 2t_2$). The electric field of this mode (TM$_{100}$ or TM$_{010}$) within the cavity is polarized along the z axis and can be approximately obtained by

$$E_z(x, y) \approx E_{z0} \cos\left(\frac{\pi n}{w}x\right) \cos\left(\frac{\pi m}{w}y\right) \approx E_{z0} \cos\left(\frac{\pi}{w}x\right)$$
$$\approx E_{z0} \cos\left(\frac{\pi}{w}y\right) \quad (3)$$

and is independent of z [49,70]. By inserting a BSCCO layer between the silicon layers, the electric field becomes localized in the superconducting region in Fig. 3(c). The enhancement of the electric field in the BSCCO region can be beneficial for the development of ultrasensitive vdW-based superconducting detectors.

The minimum frequency splitting between the upper and lower hybridized states (known as vacuum Rabi splitting) can be obtained by changing the cavity resonance frequency.

The reflection spectra of the cavity array for different cavity widths ranging $w = 30-90\,\mu$m are shown in a color-coded plot in Fig. 4(a) where w determines the detuning between the Josephson plasma frequency and the cavity mode. In the plot, cavity width is converted to the cavity frequency using Eq. (2) with $\varepsilon_{eff} = 11.56$ (permittivity of silicon). The cavity resonance frequency of $f_c = 0.49$ THz corresponds to the cavity width of $w = 90\,\mu$m, while $f_c = 1.47$ THz is for the width of $w = 30\,\mu$m. There are two resonances with specific splitting. Here, $t = 200$ nm out of 1200 nm between two gold patches is BSCCO superconducting film. Thus, the superconducting filling fraction is equal to $F = \frac{t_3}{2t_2+t_3} \sim 0.17$. Therefore, the effective permittivity of silicon/BSCCO/silicon is defined as [49]

$$\frac{1}{\varepsilon_{eff}(\omega)} = \frac{1-F}{\varepsilon_{si}} + \frac{F}{\varepsilon_{sc}(\omega)}. \quad (4)$$

The frequency of two hybridized modes is defined as

$$\varepsilon_{eff}(\omega)f_\pm^2 = \varepsilon_{si}f_c^2. \quad (5)$$

Here, f_+ and f_- are hybridized resonance frequencies of the reflection spectrum. Those are the normal modes of coupled systems. By changing f_c with cavity width, the resonance frequencies vary. The calculated resonance frequencies are shown in Fig. 4(b). It shows a good agreement with the simulation results of Fig. 4(a). Frequency splitting from Fig. 4(b) is shown in Fig. 4(c). The minimum value corresponds to the vacuum Rabi splitting which is $2\Omega_R = 0.273$ THz and occurs at $f_c = 0.62$ THz.

The value of Rabi splitting is varied not only by changing the cavity frequency (i.e., cavity width) but also by changing the superconducting BSCCO filling fraction at a fixed value of cavity width. We investigate the reflection spectra of cavity array at different filling fractions ranging from 0.041 ($t_3 = 800$ nm and $t_2 = 200$ nm) to 0.67 ($t_3 = 50$ nm and $t_2 = 575$ nm) at cavity widths of $w = 67.3\,\mu$m where the
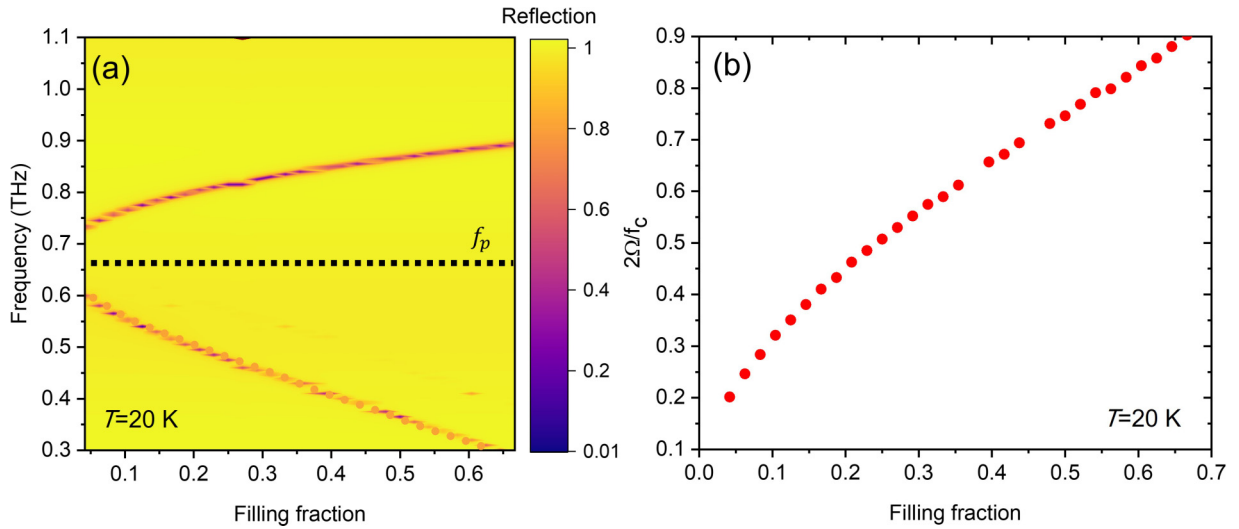
FIG. 5. (a) The color-coded reflection as a function of frequency and superconducting filling fraction $F = t_3/(2t_2 + t_3)$, where $f_c = f_p$ set in the simulation. A dotted line is passed through the data as a guide to the eye, (b) normalized Rabi splitting $2\Omega/f_c$ as a function of the filling fraction F. Here, $2t_2 + t_3 = 1.2$ μm and $w = 67.3$ μm. BSCCO thickness is varied from $t_3 = 50$ to 800 nm, which corresponds to filling fraction of 0.041 to 0.645. Here, Josephson plasma frequency is $f_p = 0.67$ THz [shown as black dashed line in (a)] at $T = 20$ K.

bare cavity resonance is equal to Josephson plasma resonance ($f_c = f_p$).

The color-coded reflection spectra are shown in Fig. 5(a). For the entire range of filling fractions, the Rabi splitting is observed. The Rabi splitting normalized to the cavity resonance $2\Omega/f_c$ [from Fig. 5(a)] is shown in Fig. 5(b). It shows a steep rise in splitting with increasing filling fraction (BSCCO thickness).

There are three regimes of weak, strong, and ultrastrong for the strength of exchange coupling between the THz EM waves and Josephson plasmons. There is a crossing between the dispersion relation of the device resonance and Josephson frequency in the case of weak coupling. A frequency splitting

and the appearance of two hybridized modes show a strong-coupling regime. When the normalized Rabi splitting is not negligible compared to 1, the system enters the so-called ultrastrong coupling regime and shows a photonic gap (splitting) in the device dispersion spectra [71,72]. Our microcavity array device goes more deeply into the ultrastrong coupling regime by increasing the superconducting filling fraction.

V. TEMPERATURE DEPENDENCE OF COUPLING STRENGTH

The active manipulation of superconducting devices originates from the Cooper pairs' sensitive response to external
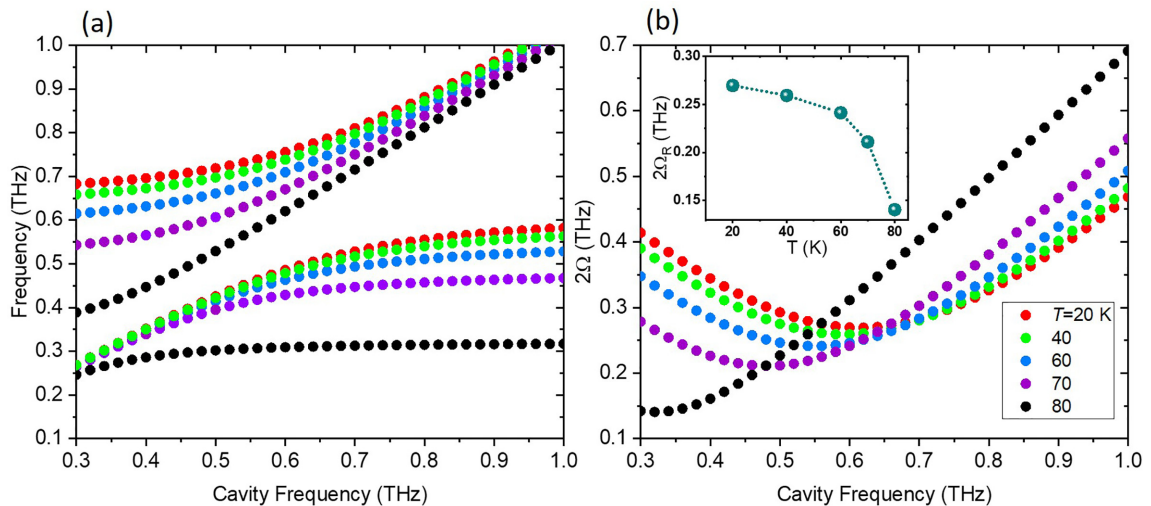
FIG. 6. (a) The theoretically calculated hybridized modes as a function of cavity frequency at different temperatures, (b) frequency splitting as a function of cavity resonance. The minimum shows the vacuum Rabi splitting. Here, BSCCO and silicon thicknesses are set to $t_3 = 200$ nm and $t_2 = 500$ nm, respectively. This corresponds to superconducting filling fraction of $F \sim 0.17$. Inset shows the vacuum Rabi splitting as a function of temperature.
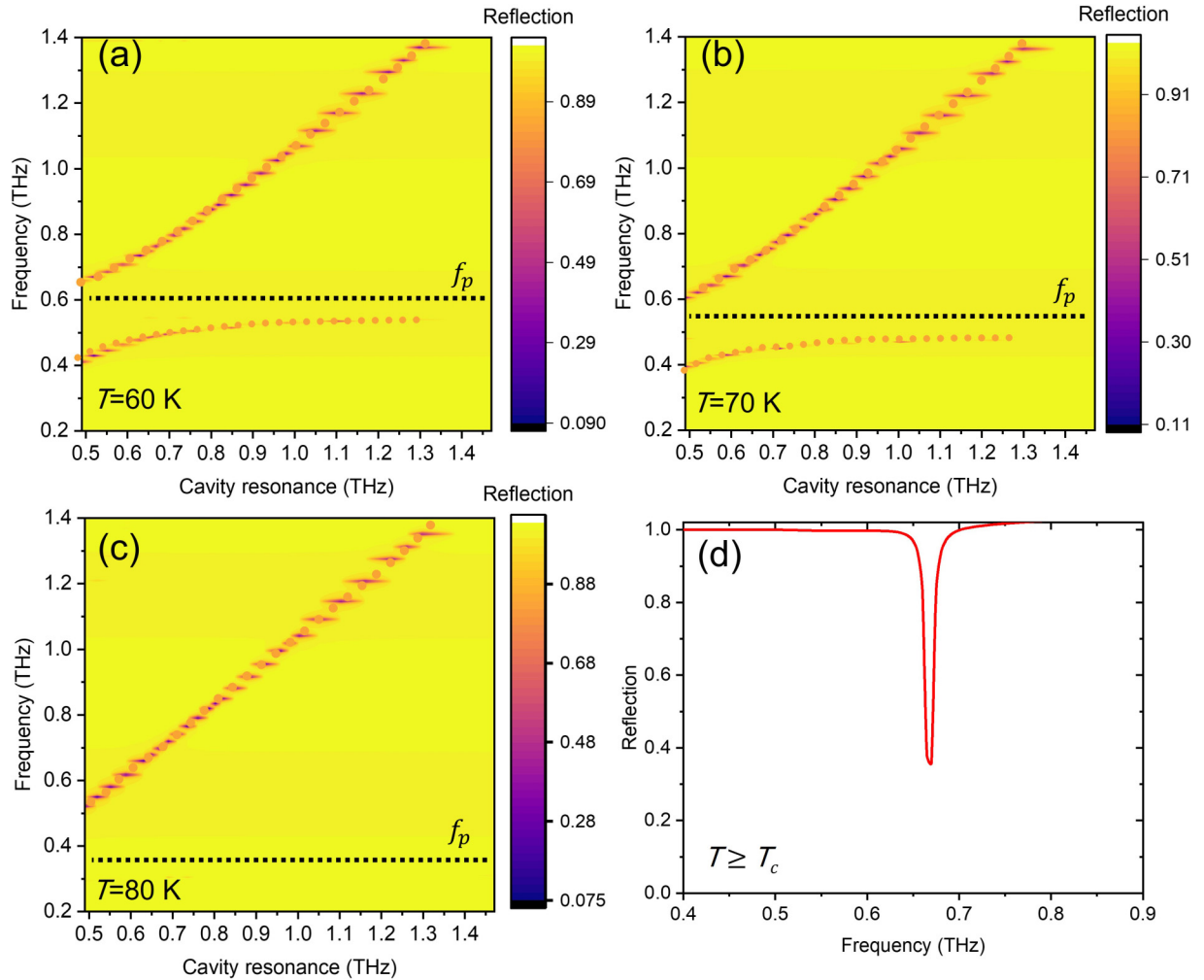
FIG. 7. The color-coded reflection as a function of frequency and cavity resonance for (a) $f_p = 0.6$ THz (representing $T = 60$ K), (b) $f_p = 0.525$ THz (representing $T = 70$ K), (c) $f_p = 0.35$ THz (representing $T = 80$ K). The cavity width w is varied from $w = 30$ to $90\,\mu$m. The black dashed line shows the Josephson plasma frequency. A dotted line is passed through the data as a guide to the eye. (d) The reflection spectra at $T \geqslant T_c$ when the cavity width is $w = 67.3\,\mu$m. Here, the thicknesses of BSCCO and silicon are set to $t_3 = 200$ nm and $t_2 = 500$ nm, with superconducting filling fraction of $F \sim 0.17$.

stimuli such as pressure, current, magnetic field, light, and temperature [73–78]. We investigate the cavity frequency detuning from the Josephson plasma frequency for different temperatures ranging $T = 20-80$ K. For this purpose, the Josephson plasma frequency at Eq. (1) is set to $f_p = 0.67$, 0.645, 0.6, 0.525, and 0.35 THz for the temperatures ranging between $T = 20$, 40, 60, 70, and 80 K, respectively [66]. Figure 6(a) shows the calculated hybridized resonance frequencies from Eqs. (4) and (5) for different temperatures when the filling fraction of the superconductor is $F \sim 0.17$ and f_c is changed from 0.3 to 1 THz. The red dots are shown earlier in Fig. 4(b). The anticrossing is observed for each temperature over its Josephson plasma frequency. The frequency splitting is extracted from Fig. 6(a) and is plotted in Fig. 6(b). It is clear that with increasing temperature the minimum splitting occurs at a lower cavity frequency.

Since the Rabi splitting is observed where the cavity resonance is tuned around the Josephson plasma resonance ($f_c = f_p$), lower Josephson plasma frequency at higher temperatures results in lower cavity resonance (smaller cavity width). The

value of minimum splitting (the vacuum Rabi splitting) is plotted in the inset of Fig. 6(b). The Rabi splitting reduces with the temperature rise as the density of the superfluid in BSCCO decreases.

The three-dimensional full-wave simulation of frequency detuning gives more insight into the effect of temperature on the coupling strength. Figures 7(a)–7(c) show the color-coded reflection spectra as a function of cavity resonance for the selected temperatures of $T = 60$, 70, and 80 K. The frequency splitting confirms the results of the simulation in Fig. 6(a). The simulation results show that the lower hybridized mode of the system gradually fades with increasing the cavity frequency. The resonance case for $f_p = 0.35$ THz (where representing $T = 80$ K) needs a cavity width of $w = 126\,\mu$m which is larger than the period of our presented microcavity array. Therefore, the lower hybridized mode cannot be illustrated in the full-wave simulation.

Figure 7(d) shows the reflection spectra at a cavity width of $w = 67.3\,\mu$m for $T \geqslant T_c$ when BSCCO is no longer in the superconducting regime. Above T_c, in the normal state,
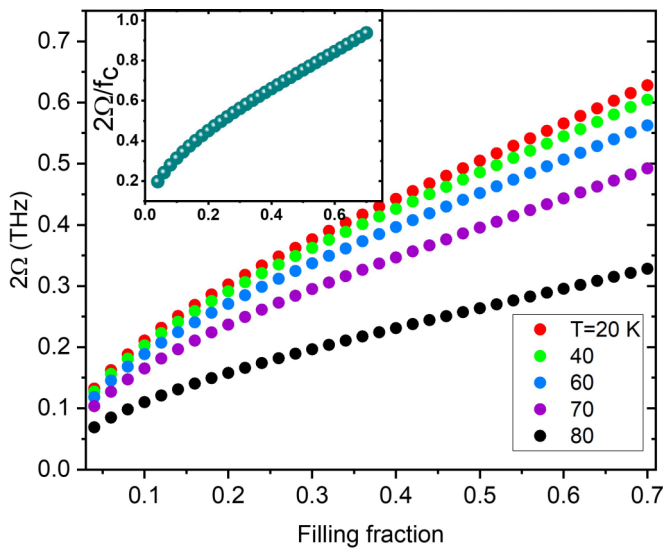
FIG. 8. The Rabi splitting $2\Omega = (f_2 - f_1)$ and (inset) normalized Rabi splitting $2\Omega/f_c$ as a function of the filling fraction F. All curves in the inset entirely overlap. Here, $2t_2 + t_3$ is set to 1200 nm. BSCCO thickness t_3 is varied from 50 to 840 nm which correspond to $F = 0.041 - 0.7$. For each curve the cavity frequency is equal to the Josephson frequency.

the charge transport of Josephson plasmon is blocked by Bi-O layers [66]. Therefore, the superconductor transport in the c-axis is like in a dielectric ($\varepsilon_{sc}(\omega) = \varepsilon_{\infty}$) and no Rabi splitting is observed. The system, therefore, enters the weak coupling regime. The reflection spectra, here, is very similar to the reflection spectra in the absence of a superconductor in Fig. 3(a). Furthermore, the effect of the filling fraction for different temperatures at the resonance condition is plotted in Fig. 8. This plot is calculated from Eqs. (4) and (5) by changing filling fraction F from 0.041 to 0.7 and $f_c = f_p$. The Rabi splitting increases with increasing the superconducting filling fraction for each temperature and it reduces with increasing the temperature. The normalized Rabi splitting $2\Omega_R/f_c$ (Rabi splitting divided by cavity resonance) is plotted in the inset of Fig. 8. It is noted that the normalized Rabi splitting is temperature independent. As long as the BSCCO material is in the superconducting regime the normalized Rabi splitting is independent of f_p [49].

VI. DISCUSSION

The strong light-matter coupling can be highly beneficial for boosting the radiated power of BSCCO IJJ THz emitters by facilitating the synchronization of Josephson current between different IJJs in BSCCO layers. Therefore, we designed an array of microcavities based on heterostructures of silicon/BSCCO/silicon to offer high resonance quality for better superconducting phase synchronization through matching of cavity resonance with Josephson frequency. In addition, our approach presents the ultrastrong light-matter coupling to lead to superconducting phase coherence through cooling the superconducting phase fluctuation. Moreover, the strong enhancement of the electromagnetic field inside the BSCCO layer also may change the electromagnetic property of the BSCCO layer itself. Indeed, the gauge-invariant phase difference φ is proportional to E/ω due to Josephson relations. This, in turn, influences the current in the layer, which is proportional to $\sin\varphi \approx \varphi - \varphi^3/6$. This affects the BSCCO refraction index $n = n_0(1 + \alpha E^2)$ with linear refraction index n_0 and strength of nonlinearity α. Such nonlinear feedback results in complicated nonlinear dynamics in the considered cavity and ultrastrong light-matter interaction which can be applied to realize power-efficient BSCCO THz source and quantum-enhanced sensitive detectors, and sensors.

VII. CONCLUSIONS

We reported a proposal for the ultrastrong coupling engineering between Josephson plasma waves of the HTS BSCCO vdW and the fundamental mode of microcavity arrays composed of silicon/BSCCO/silicon heterostructure, and demonstrated the first THz cQED. We found that the strength of coupling is adjustable by changing the proportion of superconducting film in the cavity and temperature. It is realized that Rabi splitting, as the representation of coupling, reduces with temperature increase, however, the normalized Rabi splitting is temperature independent in the superconducting state of the BSCCO with no coupling above T_c. Moreover, the light-matter interaction offered more enhancement with the increase in the superconducting filling fraction in cavity arrays. The presented ultrastrong light-matter interaction in the superconductor can lead to the development of coherent broadly tunable light sources, sensitive BSCCO THz detectors, parametric amplifiers and tunable bolometers through synchronization of Josephson current between different IJJs in BSCCO layers as a result of cooling the superconducting phase fluctuation, the high-quality of cavity resonance, and matching of Josephson frequency with cavity resonance.

[1] B. Ferguson and X. Zhang, Materials for terahertz science and technology, Nat. Mater. **1**, 26 (2002).

[2] Y. Laplace and A. Cavalleri, Josephson plasmonics in layered superconductors, Adv. Phys. **1**, 387 (2016).

[3] S. Rajasekaran, E. Casandruc, Y. Laplace, D. Nicoletti, G. D. Gu, S. R. Clark, D. Jaksch, and A. Cavalleri, Parametric ampli-

fication of a superconducting plasma wave, Nat. Phys. **12**, 1012 (2016).

[4] M. Tsujimoto, Y. Kaneko, G. Kuwano, K. Nagayama, T. Imai, Y. Ono, S. Kusunose, T. Kashiwagi, H. Minami, K. Kadowaki *et al.*, Design and characterization of microstrip patch antennas for high-T_c superconducting terahertz emitters, Opt. Express **29**, 16980 (2021).

[5] A. Dienst, E. Casandruc, D. Fausti, L. Zhang, M. Eckstein, M. Hoffmann, V. Khanna, N. Dean, M. Gensch, S. Winnerl *et al.*, Optical excitation of Josephson plasma solitons in a cuprate superconductor, Nat. Mater. **12**, 535 (2013).

[6] K. Delfanazari, H. Asai, M. Tsujimoto, T. Kashiwagi, T. Kitamura, K. Ishida, C. Watanabe, S. Sekimoto, T. Yamamoto, H. Minami *et al.*, Terahertz oscillating devices based upon the intrinsic Josephson junctions in a high temperature superconductor, J Infrared Milli. Terahz. Waves **35**, 131 (2014).

[7] K. Delfanazari, R. A. Klemm, H. J. Joyce, D. A. Ritchie, and K. Kadowaki, Integrated, portable, tunable, and coherent terahertz sources and sensitive detectors based on layered superconductors, Proc. IEEE **108**, 721 (2020).

[8] T. Kashiwagi, T. Yamamoto, T. Kitamura, K. Asanuma, C. Watanabe, K. Nakade, T. Yasui, Y. Saiwai, Y. Shibano, H. Kubo *et al.*, Generation of electromagnetic waves from 0.3 to 1.6 terahertz with a high-T_c Superconducting $Bi_2Sr_2CaCu_2O_{8+\delta}$ intrinsic Josephson junction emitter, Appl. Phys. Lett. **106**, 092601 (2015).

[9] T. Kashiwagi, M. Tsujimoto, T. Yamamoto, H. Minami, K. Yamaki, K. Delfanazari, K. Deguchi, N. Orita, T. Koike, R. Nakayama *et al.*, High temperature superconductor terahertz emitters: Fundamental physics and its applications, Jpn. J. Appl. Phys. **51**, 010113 (2012).

[10] M. Tsujimoto, H. Minami, K. Delfanazari, M. Sawamura, R. Nakayama, T. Kitamura, T. Yamamoto, T. Kashiwagi, T. Hattori, and K. Kadowaki, Terahertz imaging system using high-T_c superconducting oscillation devices, J. Appl. Phys. **111**, 123111 (2012).

[11] Y. Xiong, and K. Delfanazari, Engineering circular polarization in chip-integrated high-T_c superconducting THz antennas, in *2021 Photonics & Electromagnetics Research Symposium (PIERS)* (IEEE, 2021), pp. 1016–1019.

[12] U. Welp, K. Kadowaki, and R. Kleiner, Superconducting emitters of THz radiation, Nat. Photonics **7**, 702 (2013).

[13] K. Delfanazari, M. Tsujimoto, T. Kashiwagi, T. Yamamoto, R. Nakayama, S. Hagino, T. Kitamura, M. Sawamura, T. Hattori, H. Minami, and K. Kadowaki, THz emission from a triangular mesa structure of Bi-2212 intrinsic Josephson junctions, J. Phys. Conf. Ser. **400**, 022014 (2012).

[14] T. Kashiwagi, T. Yuasa, G. Kuwano, T. Yamamoto, M. Tsujimoto, H. Minami, and K. Kadowaki, Study of radiation characteristics of intrinsic Josephson junction terahertz emitters with different thickness of $Bi_2Sr_2CaCu_2O_{8+\delta}$ Crystals, Materials (Basel) **14**, 1135 (2021).

[15] I. Kakeya and H. Wang, Terahertz-wave emission from Bi2212 intrinsic Josephson junctions: A review on recent progress, Supercond. Sci. Technol. **29**, 073001 (2016).

[16] Y. Yu, L. Ma, P. Cai, R. Zhong, C. Ye, J. Shen, G. D. Gu, X. H. Chen, and Y. Zhang, High-temperature superconductivity in monolayer $Bi_2Sr_2CaCu_2O_{8+\delta}$, Nature (London) **575**, 156 (2019).

[17] A. K. Geim and I. V. Grigorieva, Van der Waals heterostructures, Nature (London) **499**, 419 (2013).

[18] S. Y. F. Zhao, N. Poccia, M. G. Panetta, C. Yu, J. W. Johnson, H. Yoo, R. Zhong, G. D. Gu, K. Watanabe, T. Taniguchi *et al.*, Sign-Reversing Hall Effect in Atomically Thin High-Temperature $Bi_{2.1}Sr_{1.9}CaCu_{2.0}O_{8+\delta}$ Superconductors, Phys. Rev. Lett. **122**, 247001 (2019).

[19] S. Ghosh, J. Vaidya, S. Datta, R. P. Pandeya, D. A. Jangade, R. N. Kulkarni, K. Maiti, A. Thamizhavel, and M. M. Deshmukh, On-demand local modification of high-T_c superconductivity in few unit-cell thick $Bi_2Sr_2CaCu_2O_{8+\delta}$, Adv. Mater. **32**, 2002220 (2020).

[20] M. Tsujimoto, S. Fujita, G. Kuwano, K. Maeda, A. Elarabi, J. Hawecker, J. Tignon, J. Mangeney, S. S. Dhillon, and I. Kakeya, Mutually Synchronized Macroscopic Josephson Oscillations Demonstrated by Polarization Analysis of Superconducting Terahertz Emitters, Phys. Rev. Appl. **13**, 051001 (2020).

[21] T. M. Benseman, A. E. Koshelev, V. Vlasko-Vlasov, Y. Hao, U. Welp, W. K. Kwok, B. Gross, M. Lange, D. Koelle, R. Kleiner *et al.*, Observation of a two-mode resonant state in a $Bi_2Sr_2CaCu_2O_{8+\delta}$ mesa device for terahertz emission, Phys. Rev. B **100**, 144503 (2019).

[22] K. Delfanazari, H. Asai, M. Tsujimoto, T. Kashiwagi, T. Kitamura, T. Yamamoto, M. Sawamura, K. Ishida, M. Tachiki, R. A. Klemm *et al.*, Study of coherent and continuous terahertz wave emission in equilateral triangular mesas of superconducting $Bi_2Sr_2CaCu_2O_{8+\delta}$ intrinsic Josephson junctions, Physica C: Superconductivity **491**, 16 (2013).

[23] S. Savel'ev, A. L. Rakhmanov, and F. Nori, Quantum Terahertz Electrodynamics and Macroscopic Quantum Tunneling in Layered Superconductors, Phys. Rev. Lett. **98**, 077002 (2007).

[24] S. Savel'ev, A. L. Rakhmanov, V. A. Yampol'skii, and F. Nori, Analogues of nonlinear optics using terahertz Josephson plasma waves in layered superconductors, Nat. Phys. **2**, 521 (2006).

[25] Y. Matsuda, M. B. Gaifullin, K. Kumagai, K. Kadowaki, and T. Mochiku, Collective Josephson Plasma Resonance in the Vortex State of $Bi_2Sr_2CaCu_2O_{8+\delta}$, Phys. Rev. Lett. **75**, 4512 (1995).

[26] S. Savel'ev, V. Yampol'Skii, and F. Nori, Surface Josephson Plasma Waves in Layered Superconductors, Phys. Rev. Lett. **95**, 187002 (2005).

[27] S. Savel'ev, A. L. Rakhmanov, and F. Nori, Using Josephson Vortex Lattices to Control Terahertz Radiation: Tunable Transparency and Terahertz Photonic Crystals, Phys. Rev. Lett. **94**, 157004 (2005).

[28] L. Ozyuzer, A. E. Koshelev, C. Kurter, N. Gopalsami, Q. Li, M. Tachiki, K. Kadowaki, T. Yamamoto, H. Minami, H. Yamaguchi *et al.*, Emission of coherent THz radiation from superconductors, Science **318**, 1291 (2007).

[29] K. Delfanazari, R. A. Klemm, M. Tsujimoto, D. P. Cerkoney, T. Yamamoto, T. Kashiwagi, and K. Kadowaki, Cavity modes in broadly tunable superconducting coherent terahertz sources, J. Phys. Conf. Ser. **1182**, 012011 (2019).

[30] K. Kadowaki, M. Tsujimoto, K. Delfanazari, T. Kitamura, M. Sawamura, H. Asai, T. Yamamoto, K. Ishida, C. Watanabe, S. Sekimoto *et al.*, Quantum terahertz electronics (QTE) using coherent radiation from high temperature superconducting $Bi_2Sr_2CaCu_2O_{8+\delta}$ intrinsic Josephson junctions, Phys. C (Amsterdam, Neth.) **491**, 2 (2013).

[31] K. Delfanazari, H. Asai, M. Tsujimoto, T. Kashiwagi, T. Kitamura, T. Yamamoto, W. Wilson, R. A. Klemm, T. Hattori, and K. Kadowaki, Effect of bias electrode position on terahertz radiation from pentagonal mesas of superconducting $Bi_2Sr_2CaCu_2O_{8+\delta}$, IEEE Trans. Terahertz Sci. Technol. **5**, 505 (2015).

[32] Y. Shibano, T. Kashiwagi, Y. Komori, K. Sakamoto, Y. Tanabe, T. Yamamoto, H. Minami, R. A. Klemm, and K. Kadowaki,

High-T_c superconducting THz emitters fabricated by wet etching, AIP Adv. **9**, 015116 (2019).

[33] R. Cattaneo, E. A. Borodianskyi, A. A. Kalenyuk, and V. M. Krasnov, Superconducting Terahertz Sources with 12% Power Efficiency, Phys. Rev. Appl. **16**, L061001 (2021).

[34] Y. Xiong, T. Kashiwagi, R. A. Klemm, K. Kadowaki, and K. Delfanazari, Engineering the cavity modes and polarization in integrated superconducting coherent terahertz emitters, in *2020 45th International Conference on Infrared, Millimeter, and Terahertz Waves (IRMMW-THz)* (IEEE, 2020), pp. 1–2.

[35] M. Tsujimoto, T. Yamamoto, K. Delfanazari, R. Nakayama, T. Kitamura, M. Sawamura, T. Kashiwagi, H. Minami, M. Tachiki, K. Kadowaki, and R. A. Klemm, Broadly Tunable Subterahertz Emission from Internal Branches of the Current-Voltage Characteristics of Superconducting $Bi_2Sr_2CaCu_2O_{8+\delta}$ Single Crystals, Phys. Rev. Lett. **108**, 107006 (2012).

[36] K. Delfanazari, H. Asai, M. Tsujimoto, T. Kashiwagi, T. Kitamura, T. Yamamoto, M. Sawamura, K. Ishida, C. Watanabe, S. Sekimoto *et al.*, Tunable terahertz emission from the intrinsic Josephson junctions in acute isosceles triangular $Bi_2Sr_2CaCu_2O_{8+\delta}$ mesas, Opt. Express **21**, 2171 (2013).

[37] E. A. Borodianskyi and V. M. Krasnov, Josephson emission with frequency span 1–11 THz from small $Bi_2Sr_2CaCu_2O_{8+\delta}$ mesa structures, Nat. Commun. **8**, 1742 (2017).

[38] P. Seifert, J. R. D. Retamal, R. L. Merino, H. H. Sheinfux, J. N. Moore, M. A. Aamir, T. Taniguchi, K. Watanabe, K. Kadowaki, M. Artiglia *et al.*, A high-T_c van Der Waals superconductor based photodetector with ultra-high responsivity and nanosecond relaxation time, 2D Mater. **8**, 035053 (2021).

[39] M. Li, D. Winkler, and A. Yurgens, Single-crystalline $Bi_2Sr_2CaCu_2O_{8+\delta}$ detectors for direct detection of microwave radiation, Appl. Phys. Lett. **106**, 152601 (2015).

[40] T. Tachiki, T. Uchida, and Y. Yasuoka, BSCCO intrinsic Josephson junctions for microwave detection, IEEE Trans. Appl. Supercond. **13**, 901 (2003).

[41] S. Kalhor, M. Ghanaatshoar, T. Kashiwagi, K. Kadowaki, M. J. Kelly, and K. Delfanazari, Thermal tuning of high-T_c superconducting $Bi_2Sr_2CaCu_2O_{8+\delta}$ terahertz metamaterial, IEEE Photonics J. **9**, 1 (2017).

[42] S. Kalhor, M. Ghanaatshoar, and K. Delfanazari, On-chip superconducting THz metamaterial bandpass filter, in *2020 45th International Conference on Infrared, Millimeter, and Terahertz Waves (IRMMW-THz)* (IEEE, 2020), pp. 1–2.

[43] P. Törmä and W. L. Barnes, Strong coupling between surface plasmon polaritons and emitters: A review, Rep. Prog. Phys. **78**, 013901 (2015).

[44] K. Delfanazari and O. L. Muskens, Light-Matter Interactions in Chip-Integrated Niobium Nano-Circuit Arrays at Optical Fibre Communication Frequencies, arXiv:2106.11961.

[45] K. Delfanazari and O. L. Muskens, Visible to near-infrared chip-integrated tunable optical modulators based on niobium plasmonic nano-antenna and nano-circuit metasurface arrays, in *2022 Photonics & Electromagnetics Research Symposium (PIERS)* (IEEE, 2022), pp. 924–929.

[46] H. Minami, Y. Ono, K. Murayama, Y. Tanabe, K. Nakamura, S. Kusunose, T. Kashiwagi, M. Tsujimoto, and K. Kadowaki, Power enhancement of the high-T_c superconducting terahertz emitter with a modified device structure, J. Phys.: Conf. Ser. **1293**, 012056 (2019).

[47] K. Delfanazari, H. Asai, M. Tsujimoto, T. Kashiwagi, T. Kitamura, M. Sawamura, K. Ishida, T. Yamamoto, T. Hattori, R. A. Klemm, and K. Kadowaki, Experimental and theoretical studies of mesas of several geometries for terahertz wave radiation from the intrinsic Josephson junctions in superconducting $Bi_2Sr_2CaCu_2O_{8+\delta}$, in *2012 37th International Conference on Infrared, Millimeter, and Terahertz Waves* (IEEE, 2012), pp. 1–2.

[48] T. Kashiwagi, T. Yamamoto, H. Minami, M. Tsujimoto, R. Yoshizaki, K. Delfanazari, T. Kitamura, C. Watanabe, K. Nakade, T. Yasui *et al.*, Efficient Fabrication of Intrinsic-Josephson-Junction Terahertz Oscillators with Greatly Reduced Self-Heating Effects, Phys. Rev. Appl. **4**, 054018 (2015).

[49] Y. Laplace, S. Fernandez-Pena, S. Gariglio, J. M. Triscone, and A. Cavalleri, Proposed cavity Josephson plasmonics with complex-oxide heterostructures, Phys. Rev. B **93**, 075152 (2016).

[50] C. Feuillet-palma, Y. Todorov, R. Steed, A. Vasanelli, G. Biasiol, L. Sorba, and C. Sirtori, Extremely sub-wavelength THz metal-dielectric wire microcavities, Opt. Express **20**, 29121 (2012).

[51] D. Gacemi, A. Vasanelli, L. Li, A. G. Davies, E. Lin, C. Sirtori, and Y. Todorov, Ultrastrong light − matter coupling in deeply subwavelength THz LC resonators, ACS Photonics **6**, 1207 (2019).

[52] G. S. Paraoanu, Fluorescence interferometry, Phys. Rev. A **82**, 023802 (2010).

[53] J. S. Schalch, K. Post, G. Duan, X. Zhao, Y. D. Kim, J. Hone, M. M. Fogler, X. Zhang, D. N. Basov, and R. D. Averitt, Strong metasurface–Josephson plasma resonance coupling in superconducting $La_{2-x}Sr_xCuO_4$, Adv. Opt. Mater. **7**, 1900712 (2019).

[54] D. Dietze, A. M. Andrews, P. Klang, G. Strasser, K. Unterrainer, and J. Darmo, Ultrastrong coupling of intersubband plasmons and terahertz metamaterials, Appl. Phys. Lett. **103**, 201106 (2013).

[55] Y. Todorov, A. M. Andrews, I. Sagnes, R. Colombelli, P. Klang, G. Strasser, and C. Sirtori, Strong Light-Matter Coupling in Subwavelength Metal-Dielectric Microcavities at Terahertz Frequencies, Phys. Rev. Lett. **102**, 186402 (2009).

[56] A. L. Rakhmanov, A. M. Zagoskin, S. Savel'ev, and F. Nori, Quantum metamaterials: Electromagnetic waves in a Josephson qubit line, Phys. Rev. B **77**, 144507 (2008).

[57] H. Zimmermann, *Integrated Silicon Optoelectronics* (Springer, Berlin, 2010), vol. 148.

[58] H. Chen, J. F. O. Hara, A. K. Azad, A. J. Taylor, R. D. Averitt, D. B. Shrekenhamer, and W. J. Padilla, Experimental demonstration of frequency-agile terahertz metamaterials, Nat. Photonics **2**, 295 (2008).

[59] J. Leuthold, C. Koos, and W. Freude, Nonlinear silicon photonics, Nat. Photonics **4**, 535 (2010).

[60] H. Minami, C. Watanabe, K. Sato, S. Sekimoto, T. Yamamoto, T. Kashiwagi, R. A. Klemm, and K. Kadowaki, Local SiC photoluminescence evidence of hot spot formation and Sub-THz coherent emission from a rectangular $Bi_2Sr_2CaCu_2O_{8+\delta}$ mesa, Phys. Rev. B **89**, 054503 (2014).

[61] D. P. Cerkoney, C. Reid, C. M. Doty, A. Gramajo, T. D. Campbell, M. A. Morales, K. Delfanazari, M. Tsujimoto, T. Kashiwagi, T. Yamamoto *et al.*, Cavity mode enhancement of

terahertz emission from equilateral triangular microstrip antennas of the high-T_c superconductor $Bi_2Sr_2CaCu_2O_{8+\delta}$ δ, J. Phys.: Condens. Matter **29**, 15601 (2017).

[62] R. A. Klemm, K. Delfanazari, M. Tsujimoto, T. Kashiwagi, T. Kitamura, T. Yamamoto, M. Sawamura, K. Ishida, T. Hattori, and K. Kadowaki, Modeling the electromagnetic cavity mode contributions to the THz emission from triangular $Bi_2Sr_2CaCu_2O_{8+\delta}$ mesas, Physica C: Superconductivity **491**, 30 (2013).

[63] M. Tsujimoto, T. Yamamoto, K. Delfanazari, R. Nakayama, N. Orita, T. Koike, K. Deguchi, T. Kashiwagi, H. Minami, and K. Kadowaki, THz-wave emission from inner I-V branches of intrinsic Josephson junctions in $Bi_2Sr_2CaCu_2O_{8+\delta}$, J. Phys. Conf. Ser. **400**, 022127 (2012).

[64] R. Guo, S. Duan, Z. He, X. Liang, Z. Niu, M. He, Y. Jiang, J. Wu, L. Ji, B. Jin, J. Chen *et al.*, Josephson plasmon resonance in $Tl_2Ba_2CaCu_2O_8$ high-temperature superconductor tunable terahertz metamaterials, Adv. Funct. Mater. **31**, 2106891 (2021).

[65] T. Motohashi, K. Kojima, J. Shimoyama, S. Tajima, K. Kitazawa, S. Uchida, and K. Kishio, Observation of the Josephson plasma reflectivity edge in the infrared region in Bi-based superconducting cuprates, Phys. Rev. B **61**, R9269(R) (2000).

[66] E. J. Singley, M. Abo-Bakr, D. N. Basov, J. Feikes, P. Guptasarma, K. Holldack, H. W. Hübers, P. Kuske, M. C. Martin, W. B. Peatman *et al.*, Measuring the Josephson plasma resonance in $Bi_2Sr_2CaCu_2O_{8+\delta}$ using intense coherent THz synchrotron radiation, Phys. Rev. B **69**, 092512 (2004).

[67] W. M. Haynes, D. R. Lide, and T. J. Bruno, *CRC Handbook of Chemistry and Physics*, 97th edition (Boca Raton, CRC Press, 2016-2017).

[68] S. Kalhor, S. J. Kindness, R. Wallis, H. E. Beere, M. Ghanaatshoar, R. D. Innocenti, M. J. Kelly, S. Hofmann, C. G. Smith, H. J. Joyce, and D. A. Ritchie, Active terahertz modulator and slow light metamaterial devices with hybrid graphene-superconductor photonic integrated circuits, Nanomaterials **11**, 2999 (2021).

[69] Comsol Multiphysics: Www.Comsol.Com.

[70] Y. Todorov, L. Tosetto, J. Teissier, A. M. Andrews, and P. Klang, Optical properties of metal-dielectric-metal microcavities in the THz frequency range, Opt. Express **18**, 13886 (2010).

[71] J. Pierre, A. Vasanelli, Y. Todorov, A. Delteil, G. Biasiol, L. Sorba, and C. Sirtori, Transition from strong to ultrastrong coupling regime in mid-infrared metal- dielectric-metal cavities, Appl. Phys. Lett. **98**, 231114 (2011).

[72] G. Günter, A. A. Anappara, J. Hees, A. Sell, G. Biasiol, L. Sorba, S. De Liberato, C. Ciuti, A. Tredicucci, A. Leitenstorfer, and R. Huber, Sub-cycle switch-on of ultrastrong light-matter interaction, Nature (London) **458**, 178 (2009).

[73] R. Singh and N. Zheludev, Superconductor photonics, Nat. Photonics **8**, 679 (2014).

[74] S. Kalhor, M. Ghanaatshoar, H. J. Joyce, D. A. Ritchie, K. Kadowaki, and K. Delfanazari, Millimeter-wave-to-terahertz superconducting plasmonic waveguides for integrated nanophotonics at cryogenic temperatures, Materials **14**, 4291 (2021).

[75] S. Kalhor, M. Ghanaatshoar, and K. Delfanazari, Guiding of terahertz photons in superconducting nano-circuits, 2020 Int. Conf. UK-China Emerg. Technol. UCET **2020**, 27 (2020).

[76] T. Kitamura, T. Kashiwagi, M. Tsujimoto, K. Delfanazari, M. Sawamura, K. Ishida, S. Sekimoto, C. Watanabe, T. Yamamoto, H. Minami *et al.*, Effects of magnetic fields on the coherent THz emission from mesas of single crystal $Bi_2Sr_2CaCu_2O_{8+\delta}$, Phys. C (Amsterdam, Neth.) **494**, 117 (2013).

[77] K. Delfanazari, V. Savinov, O. L. Muskens, and N. I. Zheludev, Optical superconducting plasmonic metamaterial, in *9th International Congress on Advanced Electromagnetic Materials in Microwaves and Optics – Metamaterials* (University of Southampton Institutional Repository, 2015).

[78] V. Savinov, K. Delfanazari, V. A. Fedotov, and N. I. Zheludev, Giant nonlinearity in a superconducting sub-terahertz metamaterial, Appl. Phys. Lett. **108**, 101107 (2016).